SEBHA UNIVERSITY CONFERENCE PROCEEDINGS, VOL.04 NO. 3 2025
DOI: 10.51984/SUCP.V4I3.4100

وقائع مؤتمرات جامعة سبها
Sebha University Conference Proceedings

Confrence Proceeeding homepage: http://www.sebhau.edu.ly/journal/CAS

The Non-multifractal Behavior for the Continuous Automorphism of the Torus (Cat) Map

Ibrahim Alsendid

Mathematics Department, Sebha University, 5 October Street, Sabha, Libya

Keywords:
Non-multifractal,
Dynamical systems,
Cat map,
Mixing,
Uniformal distribution.

ABSTRACT

Multifractal analysis delves into the notion that different regions within a system can exhibit distinct scaling properties, challenging the traditional concept of uniform scaling. Unlike traditional fractals, which possess a single scaling exponent, multifractals capture the heterogeneity and self-similarity present in complex systems. This allows for a more nuanced understanding of the underlying dynamics, revealing hidden patterns and uncovering the intricate interplay between order and chaos. A homogeneous set is referring to a set that is uniformly distributed. Which has no variations in density, structure, or other properties across its domain. The non-multifractal homogeneous set is a set that exhibits both non-multifractal properties and homogeneity. This means that the set displays a degree of self-similarity at a specific scale, while also having uniform distribution in its properties. The paper considers the non-multifractal properties of a map of discrete-time dynamical systems from the 2-torus to itself and how uniformly distributed global stable and unstable manifolds can be. This research employs the classical multifractal formalism to show the non-multifractal behavior of the Cat map, where the ergodicity of the map is explained. Then, theoretical multifractal functions are provided such as the cumulative curve length, the exponent D_α, the fractal dimension D_0, the dispersion $\Delta(\alpha)$, skew parameter s, and the clustering coefficient $\Delta(f)$. Lastly, the physical interpretations for the theoretical multifractal functions will be provided. Python data science is utilised to demonstrate the results.

السلوك الغير متعدد الفراكتالية لتطبيق التشاكل التقابلي الذاتي المتصل على سطح حلقي (تطبيق القطة)

إبراهيم محمد سالم الصنديد

قسم الرياضيات، جامعة سبها، شارع 5 أكتوبر، سبها، ليبيا

الكلمات المفتاحية:
متعدد الفراكتالية
الأنظمة الديناميكية
تطبيق القطة
المزج في الأنظمة الديناميكية
التوزيع المنتظم

الملخص

تحليل متعدد الفراكتالية يتعمق في مفهوم أن المناطق المختلفة داخل نظام يمكن أن تُظهر خصائص قياس متميزة، متحديًا المفهوم التقليدي للقياس المنتظم. بخلاف نظرية الفراكتال التقليدية، التي تمتلك أُسًا واحدًا للقياس، متعدد الفراكتالية تُظهر عدم التجانس والتشابه الذاتي الموجودين في الأنظمة المعقدة. هذا يتيح فهمًا أدق للديناميكيات الأساسية، ويكشف عن الأنماط الخفية والتفاعل المعقد بين النظام والفوضى. المجموعة المتجانسة تشير إلى مجموعة موزعة بانتظام، أي لا تملك كثافة مختلفة أو بنية أو خصائص أخرى في نطاقها. المجموعة المتجانسة غير متعددة الفراكتالية هي مجموعة تُظهر تجانسًا وخصائص غير متعددة الفراكتالية. هذا يعني أن المجموعة تُظهر درجة من التشابه الذاتي عند مقياس معين، كما تملك خاصية التوزيع المنتظم. هذه الورقة البحثية تعرض الخصائص الغير متعددة الفراكتالية لتطبيق أنظمة ديناميكية في زمن منفصل (تطبيق القطة)، هذا التطبيق (أو الراسم) ينقل عناصر من سطح حلقي ثنائي الأبعاد إلى نفسه، وكيف يمكن أن تكون متعدد الشعب العالمية المستقرة وغير المستقرة موزعة بانتظام. هذا البحث يستخدم الصيغة الكلاسيكية لمتعددة الفراكتالية لتوضيح سلوك الغير متعدد الفراكتالية لتطبيق القطة، حيث تم شرح خاصية الارجوية للتطبيق. بعد ذلك، تم حساب دوال متعددة الفراكتالية النظرية مثل طول المنحنى التراكمي، والبعد الفراكتلي D_0، والدالة الأسية D_α، والتشتت $\Delta(\alpha)$، ومعامل التجميع $\Delta(f)$، ومعامل الانحراف S.

* Ibrahim Alsendid:
E-mail addresses: ibr.alsendid@sebhau.edu.ly,

Article History : Received 20 February 2025 - Received in revised form 01 September 2025 - Accepted 07 October 2025

أظهرت نتائج هذه الدراسة أن العناصر (القطع المستقيمة) الموجودة على متعدد الشعب متوزعة توزيع منتظم تحت تأثير تطبيق القطة، وذلك بسبب تأثير كثافة التطبيق وتشتته وتجميعه. تعرض الدراسة التفسيرات الفيزيائية لدوال متعددة الفراكتالية. تم استخدام لغة برمجة البايثون لبناء كود وعرض النتائج.

1. Introduction

The Arnold's Cat map ('C'ontinuous 'A'utomorphism of the 'T'orus) is a chaotic map from the torus into itself, named after Vladimir Arnold. In the 1960s, Vladimir demonstrated the effects of the map using an image of a cat, hence the name [1]. Assume that the torus $\mathbb{T}^2$ is the quotient space $\mathbb{R}^2/\mathbb{Z}^2$, Arnold's Cat map is the transformation $\Gamma: \mathbb{T}^2 \longrightarrow \mathbb{T}^2$, which is composed of two maps, horizontal P and vertical Q maps, provided by: $\Gamma(x, y) = (2x + y, x + y) \bmod 1$.

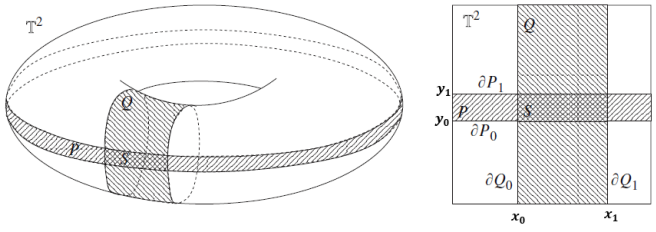

Fig. 1: The two-dimensional $\mathbb{T}^2$ with the annuli $\boldsymbol{P}$ and $\boldsymbol{Q}$. Cited in [2]

Many previous studies have examined various characteristics of the Cat map. However, this study focuses on the map's non-multifractal behavior. I am studying invariant sets of area-preserving dynamical systems. These can be computed by iterating initial conditions in forward time, that is constructing the global unstable/stable manifolds. From Ergodic theory unite tural square can be explained as follows; given $x = (p, v) \in X$, there is a unique straight line (vector) in $\mathbb{T}^2$ through the point p in the eigenvector's direction v, as shown in Fig. 2a.

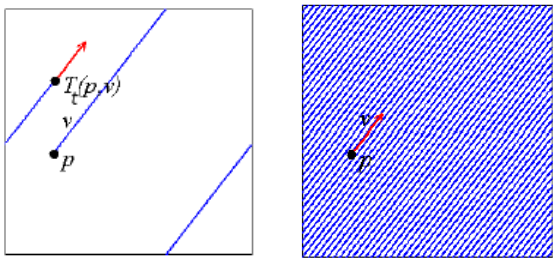

(a) (b)

Fig. 2: Plotting a vector starting from a point $\boldsymbol{p}$ in the direction $\boldsymbol{v}$.

We can extend this line infinitely in both directions by using the identifications as shown in Fig. 2b.

In principle, doing the numerical experiments by growing the unstable manifold is very easy. I could start with a collection of N points.

Ideally lying in along a line in the direction of the unstable manifold, and simply iterate all these points forward in time.

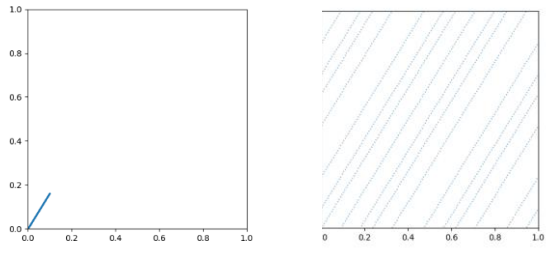

(a) (b)

Fig. 3: Numerical representations of unstable manifold at the origin of the Cat map, formed by iterating 1000 points forward 4 times

Fig. 3a shows a piece of local unstable manifold at the origin, numerically generated and consisting of $N = 1000$ points. Fig. 3b shows part of the global unstable manifold at the origin, formed by iterating the 1000 points on the local unstable manifold forward 4 times.

Fig. 3 show the results of this procedure for the map. This is numerically extremely simple, but the disadvantages are clear.

The action of the Cat map is to cause points on the unstable manifold to separate under forward iteration, at the exponential rate given by the eigenvalue λ_+ of the jacobian of the map. This means that although the local manifold in Fig. 3a may look like a solid line, the fact that it is made up of individual points appeared clear in Fig. 3b. Here, the unstable manifold has stretched to the extent that gaps are visible between points. However, the line segments are still clear.

I could improve this figure by choosing a larger number of points N, the exponential separation of points means that we have to increase N exponentially to gain a linear growth in the length of the global manifold, and this is numerically very expensive.

Bridging that research gap, this study will provide the endpoints calculation method, which is a method to numerically construct a global manifold for the Cat map.

This method relies on the piecewise linearity of the map, where an ω-measure will be employed to compute the proportion of the infinitely long unstable/stable manifold which intersects the region (measurable set), which is exactly what we do when we use box-counting methods. By studying the construction of un/stable manifolds of the map, and plotting the map, we should be able to observe whether the distribution of the line segments is uniform or non-uniform and supposedly singular.

Multifractals usually highlight the heterogeneity and self-similarity exhibited by complex systems, unlike traditional fractals that utilise a single scaling exponent. More details about the traditional fractals are provided in [3].

This article provided a numerical method to construct the Cat map. Next, a number of properties of the map are reviewed. After which, tools to investigate the uniformity of the distribution of the line-segments are provided. Then, theoretical multifractal functions are computed. As a result, the study showed that the uniform distribution of the line segments on the manifold ruled by the map has an effect on the map's density, clustering, and dispersion.

The paper is organised as follows: the forward Cat map will be introduced in section 2, where the line segments are parallel with a gradient of the eigenvector v_+ will be computed on the unstable manifold. Then, section 3 will provide the endpoints calculation method. In section 4, the backward Cat map will be introduced where the line segments are parallel with a gradient of the eigenvector v_- will be computed on the stable manifold.

In section 5, properties of the map will be reviewed, such as the hyperbolicity of the map, and then the anosov diffeomorphism and uniform hyperbolicity for the map will be explained. Moreover, the Diagonalization of the Jacobian of the map will be presented. Furthermore, an applied method to prove of the ergodicity of the map will be provided. Section 6 shows the map's non-multifractal behavior. These are tools to investigate the uniformity of the distribution of streamlines on the manifold. Lastly, in the conclusion, the physical interpretations for the theoretical multifractal functions will be provided.

2. The Forward Cat Map

The forward Cat map is composed of two maps: $F(x, y) = (x + y, y)$, $0 < y \leq 1$ and $G(x, y) = (x, x + y)$, $0 < x \leq 1$. The composition $H(x, y)$ of the above two maps is given by: $GoF = (x + y,\ x + 2y) \bmod 1,\ 0 < x, y \leq 1$. The composition H has a Jacobian $\begin{pmatrix} 1 & 1 \\ 1 & 2 \end{pmatrix}$. The eigenvalues of this Jacobian are $\lambda_\pm = (3 \pm \sqrt{5})/2$, while the eigenvectors that correspond to the map's eigenvalues are $v_\pm = \begin{pmatrix} 1 \\ \lambda_\pm - 1 \end{pmatrix}$.

The endpoints calculation method is a method to numerically constructing the global manifold, that it simply contains straight line segments of gradient given by the un/stable eigenvectors $v_\pm$. It is mainly used to compute the ω-measure and build up a code to plot out the un/stable manifold of the map, in order to study the behavior of the map.

3. Endpoints Calculation Method for the Cat Map

The endpoints calculation method is based on finding the endpoints of the line segment, which is essentially a straight line that wraps around the torus, which is dense in $\mathbb{R}^2/\mathbb{Z}^2$ due to the slope of the vector v_+ is irrational and its gradient is equal to $(1 \pm \sqrt{5})/2$. Fig. 4 shows the three different regions where the line segments on the unstable manifold connect different edges of the square; the first one connects the bottom of the square to the top, the second one from the bottom to the right-hand side, and the third one from the left-hand side to the top. Cover the manifold with a grid box, and then by simple geometry, the position of the endpoints of the line-segments can be computed, and store only these endpoints, rather than many points on the manifold. The geometry of these line segments is summarized in Table (1). In practice, the endpoints are generated by repeatedly giving a start point, then computing the corresponding endpoint via Table (1), given an endpoint, then generating the next start point according to the toral identifications of the sides of the square.

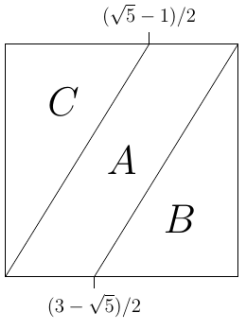

Fig. 4: Partition of the torus into regions where the unstable manifold line segments connect different edges of the square, which gives a better numerical representation of the unstable manifold at the origin for the Cat map.

Table 1: Coordinates of start and end points of line segments in the unstable manifold, in each region shown in Fig. 3.

Region	Start point	End point
A	$(x,0), x \in [0,(3-\sqrt{5})/2]$	$[x+2/(1+\sqrt{5}),1]$
B	$(x,0), x \in [(3-\sqrt{5})/2,1]$	$[1,(1+\sqrt{5})x/2]$
C	$(0,y), y \in [0,1]$	$[(\sqrt{5}-1)(1-y)/2,1]$

By building a code from the data in Table (1), we plot out the Cat map in Fig. 4.

The following improves on this method of iterating loads and loads of constituent points, using the fact that we know the gradient of the unstable manifold. Numerically, a function is defined to compute the start and end points of a global unstable manifold growing from the origin. The list "starts" contains coordinates of the start points (those on the left and bottom edges of the square), and "end" is a list of coordinates of endpoints (on the right and top edges). It repeatedly takes the last start point in the list, then uses that to find the corresponding endpoint and adds that to the ends list. Then the next start point is found by identifying the edges of the square.

The forward Cat map will be plotted by computing the line segments on the unstable manifold for H. These are simply parallel lines with a gradient $(1+\sqrt{5})/2$.

4. The Backward (Inverse) Cat Map

The backward Cat map is composed of two maps: $F(x,y)^{-1} = (x-y,y), 0 < y \leq 1$ and $G(x,y)^{-1} = (x,y-x), 0 < x \leq 1$. The composition $H(x,y)^{-1} = F^{-1}oG^{-1} = (2x-y, y-x) \bmod 1, 0 < x,y \leq 1$, has a Jacobian $\begin{pmatrix} 2 & -1 \\ -1 & 1 \end{pmatrix}$. The eigenvalues of this Jacobian are $\lambda_\pm = (3 \pm \sqrt{5})/2$, while the eigenvectors that correspond to these eigenvalues are $v_\pm = \begin{pmatrix} 1 \\ \lambda_\pm - 1 \end{pmatrix}$.

To compute the stable manifolds H^{-1} which is the inverse map of H, we write a corresponding function that simply grows the unstable manifolds for H^{-1} in the same way as above. Note that this function is not identical to the one above, as the geometry is slightly different, we should have lines of negative gradient $(1-\sqrt{5})/2$. See Fig. 5b.

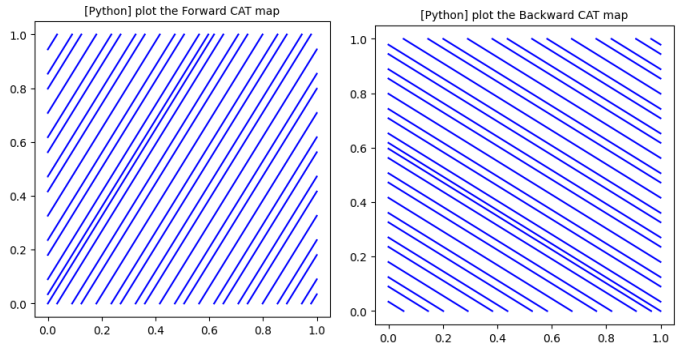

(a) (b)

Fig. 5: Plotting the Cat map using the endpoint calculation method. Fig. 5a shows the forward Cat map. While Fig. 5b shows the backward Cat map.

5. Properties of the Cat Map

5.1. The Cat Map Mixes well

Since the matrix has determinant 1, the inverse of the Cat map contains integer elements, making it invertible.

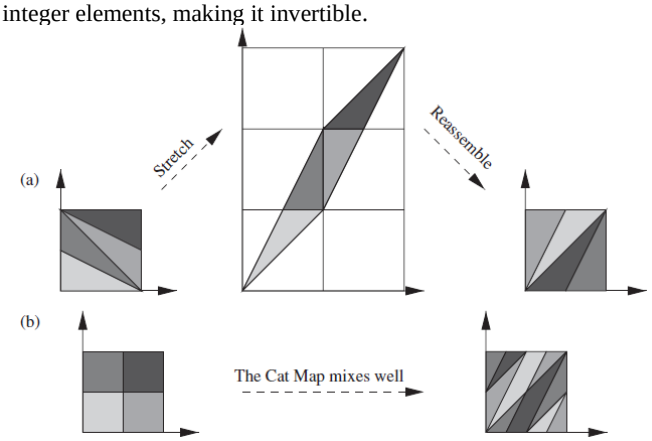

Fig. 6: The diagram cited by Sturman in [2] where (a) shows a unit square of four parts stretched and squeezed by the Cat map into the parallelogram, then re-assembled into a different shaded unit square. While (b) shows a unit square that is mixing qualities by the Cat map and shaded into quadrants.

5.2. The Hyperbolicity of the Cat Map

Definition 1: A linear map $H: \mathbb{R}^n \to \mathbb{R}^n$ is hyperbolic if all of the eigenvalues of the jacobian DH lie off the manifold (i.e. unit square torus).

For example, when $H(x,y) = (\lambda x, \mu y)$ with $0 < \lambda < 1 < \mu$, we have $DH = \begin{pmatrix} \lambda & 0 \\ 0 & \mu \end{pmatrix}$, and the eigenvalues λ and μ by definition lie off the unit square. The Cat map has a hyperbolic fixed point and it is unique, the vertices of the square.

For $\lambda_i, i = 1,2,3,\ldots,n$, the unstable (expanding) subspace E^u is defined as a subspace of $\mathbb{R}^n$ and is the span of all eigenvectors corresponding to $|\lambda_i| > 1$, which contains all vectors that are expanding under the linear map H.

The stable (contracting) subspace E^s as a subspace of $\mathbb{R}^n$ to be the span of all eigenvectors corresponding to $|\lambda_i| < 1$. E^s contains all vectors that contract under the linear map H.

E^0 is the neutral tangent space, a subspace of $\mathbb{R}^n$, and is the span of all eigenvectors corresponding to $|\lambda_i| = 1$ which contains all vectors that do not have exponential expansion or contraction under the linear map H. When $E^0 = \emptyset$ then the map H is hyperbolic.

5.3. The Diagonalization of the Jacobian of the Cat map

A matrix $D = [d_{ij}] \in M_{n,m}(F)$ is diagonal if $d_{ij} = 0$ whenever $j \neq i$. If all the diagonal entries of a diagonal matrix are positive (nonnegative) real numbers, we refer to it as a positive (nonnegative) diagonal matrix.

Definition 2: If A and B are square matrices, then we say that B is similar to A if there is an invertible matrix P such that $B = P^{-1}AP$.

Definition 3: A square matrix A is said to be diagonalizable if it is similar to some diagonal matrix; that is, if there exists an invertible matrix P such that $P^{-1}AP$ is diagonal. In this case, the matrix P is

said to diagonalize A.

A Procedure for Diagonalizing an $n \times n$ Matrix is provided by [4] :

Step 1. Determine first whether the matrix is actually diagonalizable by searching for n linearly independent eigenvectors. One way to do this is to find a basis for each eigenspace and count the total number of vectors obtained. If there is a total of n vectors, then the matrix is diagonalizable, and if the total is less than n, then it is not.

Step 2. If you ascertained that the matrix is diagonalizable, then form the matrix $P = [p_1\, p_2 \dots p_n]$ whose column vectors are the n basis vectors you obtained in Step 1.

Step 3. $P^{-1}\, A\, P$ will be a diagonal matrix whose successive diagonal entries are the eigenvalues $\lambda_1, \lambda_2, \dots, \lambda_n$ that correspond to the successive columns of P.

The Diagonalization of the Jacobian of the Cat map can be shown as follows: $A = \begin{bmatrix} 1 & 1 \\ 1 & 2 \end{bmatrix}$, the eigenvalues are $\lambda_{\pm} = (3 \pm \sqrt{5})/2$. The eigenvectors that correspond to λ_+ is $p_1 = \left(1, (1+\sqrt{5})/2\right)$. While for λ_- is $p_2 = \left(1, (1-\sqrt{5})/2\right)$. There are two basis vectors in total, so the matrix $P = \begin{bmatrix} 1 & 1 \\ \frac{1+\sqrt{5}}{2} & \frac{1-\sqrt{5}}{2} \end{bmatrix}$, So we can find

$D = P^{-1}\, AP = \begin{bmatrix} \frac{3+\sqrt{5}}{2} & 0 \\ 0 & \frac{3-\sqrt{5}}{2} \end{bmatrix}$, i.e A diagonalized by P.

Moreover, for any integer number k, $D^k = (P^{-1}\, AP)^k = P^{-1}\, A^k P$.

For example: $D^{10} = P^{-1}\, A^{10} P = \begin{bmatrix} 4181 & 6765 \\ 6765 & 10946 \end{bmatrix} = (P^{-1}\, AP)^{10}$.

5.4. Anosov Diffeomorphism and Uniform Hyperbolicity

For each point x in $\mathbb{T}^2$, denote by $E^s(x)$ and $E^u(x)$ the one-dimensional subspaces of the tangent space obtained by the translation of the eigenlines of DH. These subspaces are called the unstable and stable subspaces at x, respectively.

Definition 2: A diffeomorphism $H: M \to M$ of a compact Riemannian manifold M is Anosov if there exist constants $c > 0$, $0 < \lambda < 1$ and a continuous splitting of tangent space $T_x M = E_x^s \oplus E_x^u$ at each $x \in M$ such that:

$$(Condition1) = \begin{cases} D_x\, H\, E_x^s = E_{H(x)}^s, \\ D_x\, H\, E_x^u = E_{H(x)}^u. \end{cases} \qquad (1)$$

That is E_x^s and E_x^u should be invariant under the action of the derivative DH. Thus we take the stable subspace map to stable subspace, and the unstable subspace map into unstable subspace as we iterate the map.

$$(Condition2) = \begin{cases} \|D_x\, H^n\, v_s\| \le c\lambda^n \|v_s\| \text{ for } v_s \in E_x^s, \\ \|D_x\, H^{-n}\, v_u\| \le c\lambda^n \|v_u\| \text{ for } v_u \in E_x^u. \end{cases} \qquad (2)$$

That gives a rate of expanding for vectors $v \in E_x^u$ under forward iteration, and contraction for vectors $v \in E_x^s$ under backward iteration.

Note 1: For a differentiable map (a diffeomorphism), "uniformly hyperbolic" and "Anosov" are the same thing. They both express the idea that at every point in the space, the tangent can be split into stable and unstable directions (subspaces), with exponential contraction in the stable direction, and exponential expansion in the unstable direction (where this contraction and expansion are bound away from zero). This is the second condition (2). Moreover, the unstable and stable subspaces are invariant (this is the first condition (1)).

Note 2: If map H did not meet the condition of uniform hyperbolicity, then we say H is a non-uniformly hyperbolic map.

From the definition of Anosov diffeomorphisms in condition (2) and by assuming $c = 1$, that gives as:

$\|D\, H^{+n}\, v_-\| \le \lambda_-^{+n} \|v_-\|$ whenever $v_- \in E^s(x)$ and $n \ge 0$, (3)

$\|D\, H^{-n}\, v_+\| \le \lambda_+^{-n} \|v_+\|$ whenever $v_+ \in E^u(x)$ and $n \ge 0$, (4)

The Cat map satisfies these conditions with λ_+ and λ_- being the eigenvalues given above, with associated eigenvectors v_+ and v_-.

For the Cat map; $\|D\, H^{+n}\, v_-\| \le \lambda_-^{+n} \|v_-\|$

At $n = 1$: $\left\| \begin{pmatrix} 1 & 1 \\ 1 & 2 \end{pmatrix}^{+1} \begin{pmatrix} 1 \\ \frac{1-\sqrt{5}}{2} \end{pmatrix} \right\| = \left(\frac{3-\sqrt{5}}{2}\right)^{+1} \left\| \begin{pmatrix} 1 \\ \frac{1-\sqrt{5}}{2} \end{pmatrix} \right\|$

$$\sqrt{\left(\frac{3-\sqrt{5}}{2}\right)^2 + \left(2-\sqrt{5}\right)^2} = \sqrt{\left(\frac{3-\sqrt{5}}{2}\right)^2 + \left(1 + \left(\frac{1-\sqrt{5}}{2}\right)^2\right)} =$$

$$\sqrt{\frac{25}{2} - \frac{11\sqrt{5}}{2}}.$$

At $n > 1$: $\left\| \begin{pmatrix} 1 & 1 \\ 1 & 2 \end{pmatrix}^{+n} v_- \right\| = \left(\frac{3-\sqrt{5}}{2}\right)^{+n} \|v_-\|$

$$\Rightarrow \left\| \left(P \begin{pmatrix} \lambda_+ & 0 \\ 0 & \lambda_- \end{pmatrix} P^{-1} \right)^{+n} v_- \right\| = \left(\frac{3-\sqrt{5}}{2}\right)^{+n} \|v_-\|$$

$$\Rightarrow \left\| P \begin{pmatrix} {\lambda_+}^n & 0 \\ 0 & {\lambda_-}^n \end{pmatrix} P^{-1}\, v_- \right\| = \left(\frac{3-\sqrt{5}}{2}\right)^{n} \|v_-\|$$

Here as n goes to ∞ then ${\lambda_-}^n \to 0$, so we get:

$$\Rightarrow \|({\lambda_+}^n)\, v_-\| = \left(\frac{3-\sqrt{5}}{2}\right)^{n} \|v_-\|$$

Since $\lambda_+ = \frac{3-\sqrt{5}}{2}$. That confirm the Cat map is diffeomorphism Anosov and it is uniformly Hyperbolic.

5.5. The Lyapunov exponent for the Cat map

The Lyapunov exponent at a point x in direction v is given by:

$$\chi^{\pm}(x, v) = \lim_{n \to \pm\infty} \frac{1}{n} \log \|D\, H_x^n\, v_{\pm}\| \qquad (5)$$

whenever the limit exists. It is a straightforward calculation to show that the Cat map has the largest Lyapunov exponent given by $\log(\lambda_+)$.

Since $v_- \in E_x^s$, $v_+ \in E_x^u$, $n \ge 0$, the Lyapunov exponent for the Cat map is computed as follows;

$$D\, H^n v = \frac{-1}{\sqrt{5}} \begin{bmatrix} 1 & 1 \\ \frac{1+\sqrt{5}}{2} & \frac{1-\sqrt{5}}{2} \end{bmatrix} \begin{bmatrix} \left(\frac{3+\sqrt{5}}{2}\right)^n & 0 \\ 0 & \left(\frac{3-\sqrt{5}}{2}\right)^n \end{bmatrix} \begin{bmatrix} \frac{1-\sqrt{5}}{2} & -1 \\ \frac{-1-\sqrt{5}}{2} & 1 \end{bmatrix} \begin{pmatrix} v_1 \\ v_2 \end{pmatrix},$$

$$\|D\, H^n v\|_{L_1} = \left(\frac{3+\sqrt{5}}{2}\right)^{n+1} \times \left(\frac{\sqrt{5}-1}{2\sqrt{5}} v_1 + \frac{1}{\sqrt{5}} v_2\right) + \left(\frac{3-\sqrt{5}}{2}\right)^{n+1} \times \left(\frac{\sqrt{5}+1}{2\sqrt{5}} v_1 - \frac{1}{\sqrt{5}} v_2\right).$$

Thus; $\lim_{n \to \pm\infty} \frac{1}{n} \log \|D\, H^n\, v\| =$

$$= \lim_{n \to \infty} \frac{1}{n} \log \left(\left(\frac{3+\sqrt{5}}{2}\right)^{n+1} \times \left(\frac{\sqrt{5}-1}{2\sqrt{5}} v_1 + \frac{1}{\sqrt{5}} v_2\right) + \left(\frac{3-\sqrt{5}}{2}\right)^{n+1} \times \left(\frac{\sqrt{5}+1}{2\sqrt{5}} v_1 - \frac{1}{\sqrt{5}} v_2\right) \right).$$

$$= \lim_{n \to \infty} \log \lambda_+ + \lim_{n \to \infty} \log \lambda_- .$$

5.6. The Ergodicity of the Cat Map

For a set A and a map f, we say that A is f-invariant if $f(A) = A$, and that f is ergodic if there does not exist any splitting of the measure space $X = X_1 \cup X_2$ into two f-invariant subsets X_1 and X_2 of strictly positive measure.

The Cat map is well-known to be ergodic (a standard result that comes from the equidistribution theorem), [2] provided proof of ergodicity of the Cat map. In the applied method, the distribution of line segments on the unstable manifold generated by the Cat map is shown in Fig. 7a., where we see the gaps between the line segments. Then in Fig. 7b. the iteration time is increased until the gaps have disappeared, which illustrates ergodicity of the map. In some other cases, the gaps will never disappear if the map is not ergodic.

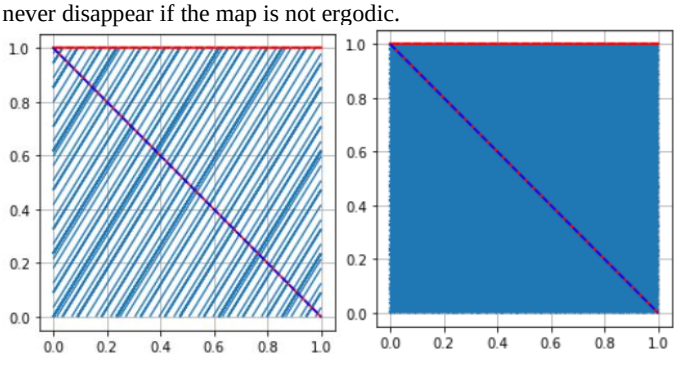

(a) (b)

Fig. 7: Ergodicity of the Cat map. Fig. 7a shows the Cat map at iteration time 5. While in Fig. 7b the Cat map at iteration time 14.

6. The Non-multifractal Behavior of the Cat Map

To study the multifractal behaviors of a map in dynamical systems, will investigate the distribution of stable and unstable leaves (i.e. the line segments) on the manifold ruled by the map in three different ways. Then will investigate the multifractal functions for the map, i.e. the generalized fractal dimension D_q, that depends on the scaling function τ_q, the partition function $Z_q(\delta)$. After which will compute the monotonic function $\alpha(q)$ and plot the singularity multifractal spectrum $f(\alpha)$. These tools essentially will provide the multifractal behaviors of the map.

6.1. The Uniformity of the Distribution of the Line segments on a Manifold Ruled by the Cat Map

1. The Probability Density Function (PDF) associated with the intersection measure μ^*:

For a cross section $\gamma = \left\{(x, y): 0 \le x < 1,\ y = \frac{1}{4}\right\}$ is a circumference. A normalized intersection measure μ^* describes the local distribution of intersection points of γ with the line-segments governed by the Cat map on the manifold.

Probability density function (PDF) associated with μ^* is given by covering a horizontal strip of the manifold with n grid boxes, such as 128 boxes, then the x-axis will be $[1, 2, 3, \ldots, 128]$. To plot the PDF function, the y-axis will be the number of line-segments inside each chamber of the grid-box. If each of these boxes has the same amount of line segments, then the PDF intersection measure will be represented as a flat histogram as shown in Fig. 8a, where the data indicate clearly that the PDFs are convergent, hence we have a uniform distribution of the line segments on the manifold. Thus the map has a non-multifractal behavior.

2. The cumulative curve associated with the intersection measure μ^*:

The cumulative curve associated with μ^* is given by the cumulative curve of the intersections of the unstable leaves with the cross-section $y = 1/4$, which is computed by covering the horizontal curve $y = 1/4$ with n grid boxes, such as 128 boxes. Then the x-axis will be $[\,1/128, 2/128, 3/128, \ldots, 128/128\,]$, while the y-axis is a list of the cumulative curve of the intersection points of the cross-section $y = 1/4$ with the line segments inside each chamber of the grid-box as shown in Fig. 8b.

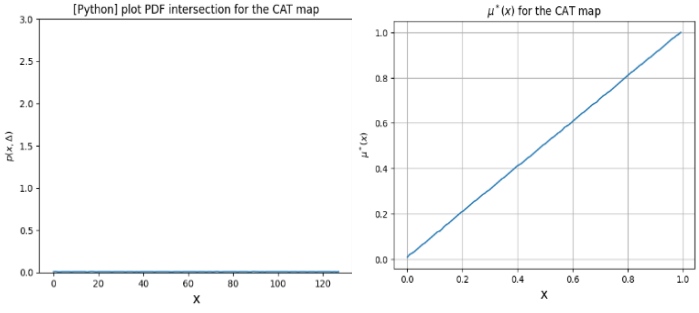

(a) (b)

Fig. 8: Fig. 8a shows the histogram of the PDF functions for the unstable Cat map at a numerical iteration time = 14. Fig. 8b shows the cumulative curve for the unstable Cat map at a numerical iteration time = 14.

In geometry, consider the cumulative curve in Fig. 8b as the length of hypotenuse, and x-axis and y-axis represent lengths of the triangle's other two sides, each one equal 1. Then from the Pythagorean theorem, the hypotenuse 's length is equal to the sum of squares of the other two sides' lengths, which gives us $\sqrt{2}$. Thus in the case of the Cat map, the distribution of the un/stable leaves (line segments) is a uniform distribution, and the length of the cumulative curve in Fig. 8b is $\sqrt{2} = 1.41421$.

3. The intersection between the stable and unstable manifolds of the Cat map:

The third tool is the measure given by the intersection of the unstable manifold with the stable manifold for the forward and backward Cat maps respectively. we consider the intersections of these sets of lines and find the intersection of a pair of lines (which are given by their endpoints), then we observe the uniformity of the distribution of intersection points, where it is clear from Fig. 9b.

6.2. The Classical Multifractal Formalism

The classical multifractal formalism is the theoretical multifractal measure generated by p-model, we use the multinomial theory to compute the multifractal functions.

The method is clearly explained by Stephen Lynch in [5], where the multifractal dimension is the generalized fractal (box-counting) dimension that works by covering a measurable set with a minimum number of boxes with size length δ (with no overlap if possible).

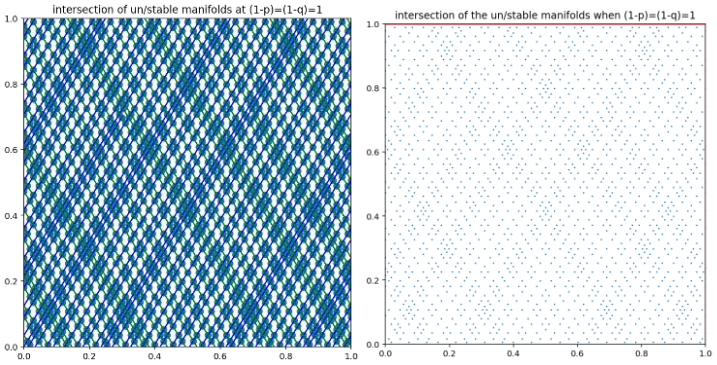

(a) (b)

Fig. 9: Distribution of the intersection points of the un/stable manifolds of the Cat map. Fig. 9a shows the intersection of un/stable manifolds that are presented in Fig. 5. The intersection points are plotted in Fig. 9b.

In this way, the box-counting dimension will be obtained from the limiting gradient, as δ goes to zero. More details in [6].

Let us assume $S \subset \mathbb{R}^d$ is an object and μ is a (self-similar) probability measure defined on S. Let $B_i(l)$ be a cover of boxes of length size l, where i is an index. The probability measure $\mu(B)$ is determined by covering S with a grid of $B_i(l)$ where i is from 1 to N, the number of boxes is indicated by $N \propto \frac{1}{l^2}$.

For $q \in \mathbb{R}$, $n = 1,2$, if we cover the object S with $N(\delta) = n^k$ of balls of diameter $\delta = l^k$, where k is the iteration time 0,1,2,…

The Scaling function $\tau(q)$ is a decreasing real analytic function from $\mathbb{R} \longrightarrow \mathbb{R}$, and given by the following formula:

$$\tau(q) = D_q(1-q) = \lim_{\delta \to 0} \frac{\ln Z_q(\delta)}{-\ln \delta}, \qquad (6)$$

$Z_q(\delta)$ is the partition function which given by:

$$Z_q(\delta) = \sum_{i=1}^{2} p_i^q(\delta) = (p_1^q + p_2^q)^k, \qquad (7)$$

where D_q is the generalized fractal dimension.

We also calculate the measure μ by covering the object by $(N_i(\delta))_{i=1}^N$ boxes with size δ, then find $p_i(\delta) = \mu\big(N_i(\delta)\big) = \mu_i$ the box measures. The normalized probabilities $\mu_i(q, \delta)$ is given by;

$$\mu_i(q, \delta) = \frac{{p_i}^q(\delta)}{\sum_{i=1}^N {p_i}^q(\delta)}. \qquad (8)$$

This allows us to compute the monotonic function $\alpha(q)$ and the spectrum $f(q)$ using the multinomial theory as follows;

$$\forall q \in \mathbb{R}, \alpha(q) = \lim_{\delta \to 0} \frac{\sum_{i=1}^N \mu_i(q, \delta) \ln p_i(\delta)}{\ln \delta}, \qquad (9)$$

$$f(q) = \lim_{\delta \to 0} \frac{\sum_{i=1}^N \mu_i(q, \delta)\ \ln \mu_i(q, \delta)}{\ln \delta}. \qquad (10)$$

6.3. Analytical Computing for the Multifractal Functions for the Cat Map

Suppose the unstable manifold of the Cat map is uniformly distributed, then:

Lemma 1: The unstable manifold for the Cat map has $D_q = 2\ \forall q$ and $f(q) = \alpha(q) = 1\ \forall q$.

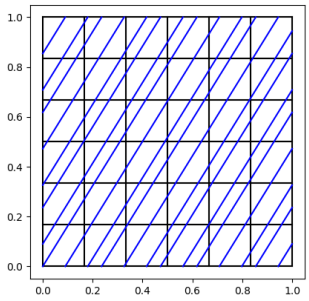

Fig. 10: Here we cover the torus with $\boldsymbol{n} \times \boldsymbol{n}$ boxes

Proof: We cover the torus with $\boldsymbol{n^2}$ boxes of side $\delta = \frac{1}{n}$.

Since the unstable manifold is uniformly distributed, the length function in each box is $p_i = \frac{1}{n^2}$,

Then the partition function $Z_q = \sum_{i=1}^{n^2} {p_i}^q = n^{2(1-q)}$ and we have

$$\tau(q) = \lim_{n\to\infty} \frac{\log Z_q}{\log n} = 2(1-q).$$

The generalised dimension $D_q = \frac{\tau(q)}{1-q} = 2, \forall q$, as the unstable manifold cover the whole torus uniformly.

The normalised probabilities $\mu_i(q,\delta)$ are given by

$$\mu_i(q,\delta) = \frac{{p_i}^q(\delta)}{\sum_{i=1}^{n^2} {p_i}^q(\delta)} = \frac{n^{-2q}}{n^{2(1-q)}} = n^{-2} (= p_i).$$

Then

$$f(q) = \alpha(q) = \lim_{\delta\to 0} \frac{\sum_{i=1}^{n^2} \mu_i \log \mu_i}{\log n^{-2}} = \frac{\sum_{i=1}^{n^2} n^{-2} \log n^{-2}}{\log n^{-2}} = 1$$

6.4. The Asymptotic Scaling Behavior of the Spectrum $f(\alpha)$

By determining α_q as a singularity exponent and f_q a density exponent, and for any given $q \in \mathbb{R}$, the construction of the spectrum $f(\alpha)$ has two labels, L(left) where $q \in \mathbb{R}_+$, and R(right) where $q \in \mathbb{R}_-$, the domain of $f(\alpha)$ is α_q. The spectrum $f(\alpha)$ expectedly contracts to the leftmost and rightmost points on the spectrum.

$f(\alpha)$ approaches f_{min} (i.e., the minimum of f_q) from both sides: the leftmost point where the domain of $f(\alpha)$ is α_{min} and q tends to $(+\infty)$, and the rightmost point where the domain of $f(\alpha)$ is α_{max} and q tends to $(-\infty)$. See Fig. 11.

The $f(\alpha)$-spectra among groups showed distinctively different shapes and symmetry. The curvature and the symmetry of the $f(\alpha)$-spectra provide information on the heterogeneity of a system, which is defined by the diversity of scaling exponents required to characterize it, which is highly associated with D_0, $\alpha(0)$, and D_1.

These functions represent the behavior at or around the maximum point of the $f(\alpha)$-spectra.

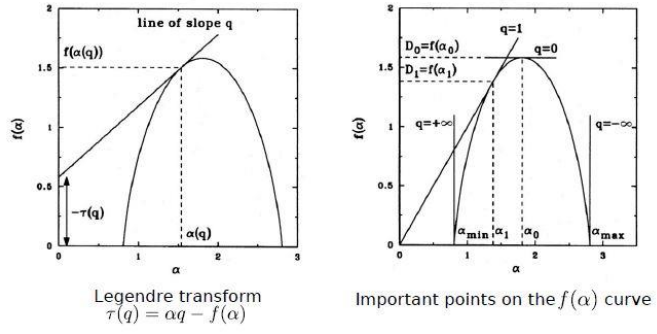

Fig. 11: The relation between the Multifractal Functions. Cited in [7]

6.5. Physical Interpretations for the Theoretical Multifractal Functions

By computing the numerical spectrum of singularity $f(\alpha(q))$ can be obtained from the Legendre transformation as follows;

$$f(\alpha(q)) = q\,\alpha(q) + \tau(q) \qquad (11)$$

we compute the density (height of the $f(\alpha)$ curve) [8], the dispersion (width of the $f(\alpha)$ curve) $\Delta\alpha = \alpha_{max} - \alpha_{min}$ [9-10], the clustering coefficient $\Delta f = f(\alpha_{min}) - f(\alpha_{max})$ [8], and the Skewed parameter $s = \frac{\alpha_{max} - \alpha_0}{\alpha_0 - \alpha_{min}}$ [11-13].

7. Conclusion

The paper mainly provided the endpoints calculation method, which is based on finding the images of the endpoints of the line segments (straight lines wrap around the torus) ruled by the map, which is dense in $\mathbb{R}^2/\mathbb{Z}^2$ due to the irrational slope of the eigenvectors. In the case of the Cat map, three different regions are proposed in which the unstable manifold line segments connect different edges of the square. We cover the manifold with a grid box, and then we compute the endpoints of the line-segments' images using simple geometry and store only these endpoints rather than many points on the manifold.

In this research, the classical multifractal formalism is employed to investigate the non-multifractal behavior of the Cat map, and a careful computational approach was utilised to show the results using Python data science.

The behavior of the map was studied in section 6 in two ways, firstly by investigating the uniform distribution of the line segments on the manifold. Then by computing the theoretical multifractal functions for the map. The curve of the generalized fractal dimension D_q is essentially constant for all q. While the physical interpretations for the theoretical multifractal functions are shown by figuring out the numerical spectrum $f(\alpha)$, where the non-multifractal of the map is determined when the width of the $f(\alpha)$ spectrum is zero, i.e., the distance between $\alpha_{max} - \alpha_{min} = 0$.

The Cat map displayed an exactly homogeneous dispersion, with the smallest value $\Delta\alpha = \Delta f = 0$ and $\alpha_0 = D_0 = s = 1$.

The results of the research show that the uniform distribution of line-segments on the manifold ruled by the Cat map influences the map's density, dispersion, and clustering.

8. Appendix

The Python code utilised to conduct the numerical analysis and plot the forward and the backward of the Cat map is available at https://github.com/IbrahimAlsendid/Classic-multifractals.git

9. References

[1]- Arnold, V. I., and Avez, A. (1968). Ergodic problems of classical mechanics, vol. 9, Benjamin.

[2]- Sturman, R., Ottino, J. M., & Wiggins, S. (2006). The mathematical foundations of mixing: the linked twist map as a paradigm in applications: micro to macro, fluids to solids (Vol. 22). Cambridge University Press.

[3]- Alsendid, I. M. (2018). Using fractal dimensions to measure the length of the coastline of Tripoli (modern method to collecting data). Journal of Pure & Applied Sciences, 17(1).

[4]- Anton, H., & Rorres, C. (2013). Elementary linear algebra: applications version. John Wiley & Sons.

[5]- Lynch, S. (2018). Dynamical systems with applications using python. Basel, Switzerland: Birkhäuser.

[6]- Alsendid, I., and Sturman, R., (2024). Multifractal properties of a family of non-monotonic toral mixing maps [Manuscript submitted for publication]. SIAM Journal on Applied Dynamical Systems.

[7]- Jones, B., 2018. Fractal and multifractal symmetries: Understanding andinterpreting fractals. URL: https://www.rug.nl/research/vsi/events/qu8/talks/qu8mc_jones.pdf.

[8]- Evans, A., Slate, A. J., Tobin, M., Lynch, S., Wilson Nieuwenhuis, J., Verran, J., ... & Whitehead, K. A. (2022). Multifractal analysis to determine the effect of surface topography on the distribution, density, dispersion and clustering of differently organised coccal-shaped Bacteria. Antibiotics, 11(5), 551.

[9]- Koscielny-Bunde, E., Kantelhardt, J. W., Braun, P., Bunde, A., & Havlin, S. (2006). Long-term persistence and multifractality of river runoff records: Detrended fluctuation studies. Journal of Hydrology, 322(1-4), 120-137.

[10]- Gimenez, D., Posadas, A., & Cooper, M. (2010, May). Multifractal Characterization of Soil Pore Shapes. In EGU General Assembly Conference Abstracts (p. 10649).

[11]- Wickens, D., Lynch, S., West, G., Kelly, P., Verran, J., & Whitehead, K. A. (2014). Quantifying the pattern of microbial cell dispersion, density and clustering on surfaces of differing

chemistries and topographies using multifractal analysis. Journal of Microbiological Methods, 104, 101-108.
[12]- Gould, D. J., Vadakkan, T. J., Poché, R. A., & Dickinson, M. E. (2011). Multifractal and lacunarity analysis of microvascular morphology and remodeling. Microcirculation, 18(2), 136-151.
[13]- Chen, Z. W., Lai, J. K. L., & Shek, C. H. (2005). Multifractal spectra of scanning electron microscope images of SnO2 thin films prepared by pulsed laser deposition. Physics Letters A, 345(1-3), 218-223.